A HIGH-CURRENT ELECTROTHERMAL BISTABLE MEMS RELAY

Jin Qiu[1] (Room 3-470, jqiu@mit.edu), Jeffrey. H. Lang[1], Alexander H. Slocum[1], Ralf Strümpler[2]
1: Massachusetts Institute of Technology, 77 Massachusetts Avenue, Cambridge, MA 02139, USA
2: ABB Corporate Research Ltd, 5404 Baden-Dättwil, Switzerland

ABSTRACT

This paper reports the design, fabrication and testing of a thermally-actuated bistable MEMS relay. Mechanical bistability ensures zero actuation power in both the on and off states, and permits actuation with a transient thermal actuator. In the off state, this relay stands off more than 200 V. In the on state, it exhibits a minimum total resistance of 60 mΩ and a maximum current carrying capacity of 3 A. It switches with a maximum 5 Hz rate.

INTRODUCTION

The development of MEMS relays has attracted considerable attention in recent years. Relays have been fabricated through surface [1,3,4,5] and bulk [2,6] micromachining, have employed electrical [2,5], magnetic [3,6] and thermal [1,4] actuation, have employed monostable [1,2,4,5,6] and bistable [3] structures, and have employed lateral [1,4] and vertical [2,3,5,6] moving contacts. One relay has employed liquid metal movement [4]. The applications have ranged from signal [1,3,4] to power [2,5,6] switching. For power switching requirements, the lowest reported on-state resistance is 14 mΩ [2] and the highest reported current-carrying capacity is several Amperes [5].

The relay reported in this paper is a bulk micromachined thermally-actuated bistable lateral relay for power applications. The bulk micromachined structure ensures good thermal diffusion at the relay contact, which together with a low contact resistance, contributes to a high current-carrying capacity. Compared with other actuators, the thermal actuator has a larger force and stroke, and requires a lower driving voltage. When coupled with a bistable relay, the disadvantage of high power required for thermal actuation is minimized by the small transient energy consumed during the actuation of a bistable relay.

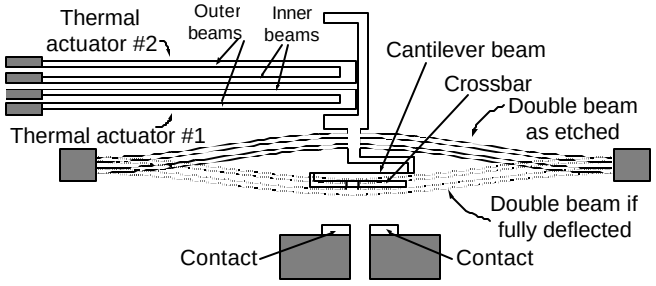

Figure 1: Plan view of the relay components.

Figure 1 shows the relay plan view, with shaded areas anchored to a handle wafer. The main components of the relay are through-etched by DRIE of a silicon wafer. At the center is a mechanically bistable pre-curved double beam [7] that moves laterally in the wafer plane. A crossbar is attached to the double beam by a cantilever beam. When the double beam is in its as-etched position (solid lines) the two contacts below the crossbar are not connected, and the relay is off. When the double beam snaps toward its second stable position (dashed lines), it pushes the crossbar against the two contacts, and the relay is on, as shown in Figure 2. Good electrical contact is ensured through metal deposited on the etched sidewalls; flat contacts have experimentally proven to give the best electrical contact. Thermal actuator #1 in Figure 1 deflects downward to close the relay. Thermal actuator #2 deflects upward to open the relay.

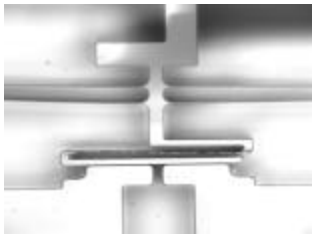

Figure 2: Microscope picture of closed contacts.

DESIGN OF THE CONTACT STRUCTURE

The bistable double beam employed in the relay is 12 μm thick, 4 mm long, 300 μm wide, and has an apex height of 72 μm. From the modeling in [7], it has the center force-displacement characteristic shown in Figure 3. This characteristic has been verified experimentally [7].

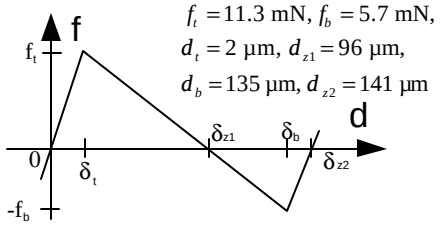

Figure 3: The bistable double beam center f-d characteristic.

The double beam should provide a total contact force of 4 mN within the 6-μm region between δ_b and δ_{z2} so as to guarantee low contact resistance. However, photolithography and DRIE etching can typically produce an etched channel width variation of about 4 μm. Such a variation causes a large variability in contact force and may even prevent contact. Inclusion of a cantilever beam having 12-μm thickness and 0.5-mm length as shown in Figure 1 solves this problem. With this extra compliance, the contact force variance is reduced to 0.6 mN. The cantilever beam is also important for balancing the force on each contact as well as for conforming the crossbar to the contacts when opposite contact sidewalls are not vertically or horizontally

parallel. Both the double beam and the cantilever beam determine the distance between the initial position of the crossbar and the contacts. To have the desired contact force of 4 mN, their separation is designed to be 137 μm.

MECHANICAL MODELING AND DESIGN OF THE ELECTROTHERMAL ACTUATOR

The bistable double beam requires thermal actuation with 13 mN of maximum force and 120 μm of stroke. These requirements are bigger than shown in Figure 3 due to the etch gap between the actuator and the double beam. To meet these requirements, while minimizing actuator size and temperature rise, a closed-form mechanical model is constructed to facilitate actuator design.

As a precursor to model development, consider the deflection of a single beam that is clamped at one end ($x=0$), free at the other end ($x=l$), yet compressed by axial force p, and deflected horizontally by force f and counterclockwise moment m applied at the free end. The horizontal bending of the single beam is described by

$$EIv'' = p(d-v)+m+f(l-x) \tag{1}$$

where E is the Young's modulus, I is the beam moment of inertia, v is the horizontal displacement, d is the tip displacement, l is the length of the beam, and x is the axial coordinate. The tip rotation is

$$q = v'_{x=l} \tag{2}$$

To clarify the analysis, define the normalized thickness

$$T = t/l \tag{3}$$

and the normalized variables

$$X = x/l,\ V = v/t,\ \Delta = d/t,\ \Theta = ql/t$$
$$K^2 = pl^2/(EI),\ M = ml^2/(EIt),\ F = fl^3/(EIt) \tag{4}$$

With these normalizations, (1) takes the form

$$V'' = K^2(\Delta - V) + M + F(1-X) \tag{5}$$

The solution of (5) is

$$V = F[\sin(KX) - \tan K\cos(KX) + \tan K - KX]/K^3 + M[1-\cos(KX)]/(K^2\cos K) \tag{6}$$

which gives a constitutive relation at the tip of

$$\Delta = c_{\Delta F}(K)F + c_{\Delta M}(K)M \tag{7}$$
$$c_{\Delta F}(K) = [\tan K - K]/K^3$$
$$c_{\Delta M}(K) = [1-\cos K]/(K^2\cos K)$$

and

$$\Theta = c_{\Theta F}(K)F + c_{\Theta M}(K)M \tag{8}$$
$$c_{\Theta F}(K) = (\sin K\tan K + \cos K - 1)/K^2$$
$$c_{\Theta M}(K) = \tan K/K$$

From Hooke's law, the beam compression strain is

$$e = K^2T^2/12 \tag{9}$$

With a small deflection assumption, the ratio of the axial beam tip movement in the negative direction to the beam length is

$$h = e + T^2\int_0^1 0.5(V'')^2\,dX = e + T^2[c_{hF}(K)F^2 + c_{hM}(K)M^2 + c_{hFM}(K)FM] \tag{10}$$

$$c_{hF}(K) = (2K\cos^2 K - 3\sin K\cos K + K)/(4K^5\cos^2 K)$$
$$c_{hM}(K) = (-\sin K\cos K + K)/(4K^3\cos^2 K)$$
$$c_{hFM}(K) = (2\cos^2 K + K\sin K - 2\cos K)/(2K^4\cos^2 K)$$

We can now consider the thermal actuator to be a combination of two beams, with analytic notation defined in (3)-(10). Let the subscripts 1 and 2 denote the individual beams with hot beam 1 to the positive-deflection side of cold beam 2. The deflection of the beam pair is as described in (5) through (10) with coupled boundary conditions at $X=1$. To continue the analysis, define

$$L_2 = l_2/l_1 \tag{11}$$
$$T_0 = t_g/l_1 + (t_1+t_2)/(2l_1) \tag{12}$$

where t_g is the gap between the two beams. The thermal strain difference between the two beams is

$$e_a = aT_{rise} \tag{13}$$

where a is the thermal expansion rate and T_{rise} is the average temperature difference. Next, the two axial forces must have equal value but opposite sign so that

$$K_2 = K_1\sqrt{-E_1I_1L_2^2/(E_2I_2)} \tag{14}$$

Further, the moment and force relation at the tip of the actuator is

$$M_1 + M_2E_2I_2T_2/(E_1I_1T_1L_2) + K_1^2T_0/T_1 = 0 \tag{15}$$

According to (7) and (8), the constitutive behavior of both beam tips is described by

$$c_{\Delta F1}(K_1)F_1 + c_{\Delta M1}(K_1)M_1 - \Delta_1 = 0 \tag{16}$$
$$c_{\Delta F2}(K_2)F_2 + c_{\Delta M2}(K_2)M_2 - \Delta_2 = 0 \tag{17}$$
$$c_{\Theta F1}(K_1)F_1 + c_{\Theta M1}(K_1)M_1 - \Theta_1 = 0 \tag{18}$$
$$c_{\Theta F2}(K_2)F_2 + c_{\Theta M2}(K_2)M_2 - \Theta_2 = 0 \tag{19}$$

The geometric constraints of the two beam tips are

$$\Theta_1 - (T_2/T_1)\Theta_2 = 0 \tag{20}$$
$$\Delta_1 - (L_2T_2/T_1)\Delta_2 = 0 \tag{21}$$
$$e_a - h_1 + L_2h_2 + T_1^2T_0\Theta_1 = 0 \tag{22}$$

Combing (9), (10) and (22) gives

$$e_a - K_1^2T_1^2/12 + L_2K_2^2T_2^2/12 + T_1^2T_0\Theta_1 - T_1^2[c_{eF1}(K_1)F_1^2 + c_{eM1}(K_1)M_1^2 + c_{eFM1}(K_1)F_1M_1] + L_2T_2^2[c_{eF2}(K_2)F_2^2 + c_{eM2}(K_2)M_2^2 + c_{eFM2}(K_2)F_2M_2] = 0 \tag{23}$$

Assuming a given K_1, (14) gives K_2, and then (15)-(21) are linear equations which can be summarized by

$$(F_1, M_1, \Delta_1, F_2, M_2, \Delta_2, \Theta_2)^T = Q_1\Theta_1 + Q_2 \tag{24}$$

Here, Q_1 and Q_2 are both 7-element vector functions of K_1. Substitution of (24) into (23) gives a quadratic equation,

$$s_1(K_1)\Theta_1^2 + s_2(K_1)\Theta_1 + s_3(K_1) + e_a = 0 \tag{25}$$

that can be solved for Θ_1. Given Θ_1, (24) then gives solutions for all other variables.

Returning to dimensional form, (4) gives

$$d_{actuator} = \Delta_1 t_1 \tag{26}$$

From a force balance and (4)

$$f_{actuator} = f_1 + f_2 = F_1E_1I_1t_1/l_1^3 + F_2E_2I_2t_2/l_2^3 \tag{27}$$

Note that (26) and (27) together give the force-displacement characteristic of the thermal actuator, parametrically over K_1. Therefore, varying K_1 in a reasonable range sweeps the trajectory of the actuator force-displacement characteristic. A zero force gives the free displacement of the actuator; a zero displacement gives the blocked force of the actuator.

A parameter design study optimized the actuator dimensions to best meet the actuation requirement. The resulting actuator is 6 mm long, with inner beams 80 µm thick, outer beams 60 µm thick, and a gap between them 20 µm wide. An average temperature difference of 220 C between the two beams is required to provide the expansion difference. Figure 4 shows a comparison of results from the model and from FEA. A MatLab implemention of the model gives a result in 2 seconds, while the construction and running of an FEA model usually takes more than a half hour for a specific design.

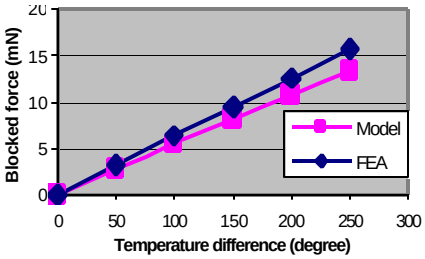

Figure 4: Thermal actuator blocked force.

The mechanical model shows that the buckling of the hot beam, which is much more severe when the hot beam is thinner than the cold beam, decreases the effective expansion difference between the two beams and limits actuator performance. This forces a design in which the thicker beam is heated. To achieve this, the colder outer beam of both actuators is covered by metal to make it more conducting than the thinner inner beam. This permits a differential heating and expansion of the beams as an electrical current is passed around them to produce the desired deflection of each actuator.

Unlike many thermal actuators [8,9], the actuator described here is a transient actuator. Correspondingly the electrical excitation is applied for only a short time. In this way, uniform temperature is maintained inside the inner hot beam and little heat flows into the outer cold beam, so the maximum expansion difference between the beams is obtained. If left excited for more than several ms, the temperatures of the two beams partially equilibrate and the actuator retracts. With a device wafer resistivity of 0.005 Ω-cm, a 1-ms 30-V pulse delivering 50 mJ is able to change the relay state. Because we used wafers with a larger resistivity than this value, our fabricated devices require a higher voltage, or a longer actuation time to drive.

FABRICATION AND TEST

The MEMS relay shown in Figures 1 and 2 has been fabricated and successfully tested. The N-type 4-inch silicon wafer used for fabrication has a 0.008-0.2 Ω-cm resistivity, and a 315-µm thickness. The 4-inch Pyrex handle wafer has a 500-µm thickness. In the etch masks for the silicon through etch, fillets are added at the sharp corners to lower stress concentration. Further, a halo is included in the mask, so that the etch space has the same width throughout the mask. This arrangement ensures that etching occurs at the same rate at all locations.

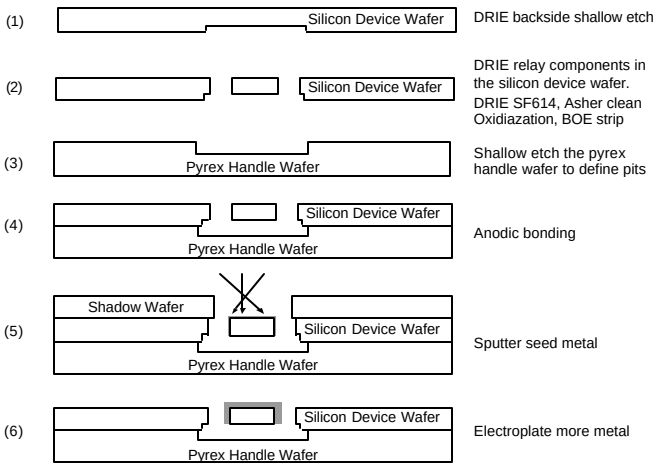

Figure 5: Fabrication process flow.

Fast-turnaround and economic mask printing was adopted for fabrication. The mask pattern was first printed on a transparency by a commercial service with a feature resolution of about 5 µm. Then the transparency pattern was transferred to a resist-covered chrome glass plate by photolithography. Finally the chrome plate was etched and cleaned, ready to be used as a mask. The time required to turn a mask drawing into a real mask is two days. For better resolution than 5 µm, a stepper exposure process can be used, which has a 10:1 feature reduction capability from the mask onto the wafer. This improves the resolution by a factor of ten.

Figure 5 shows the main fabrication process steps for the relay. First, a backside shallow pit of about 20 µm is etched by DRIE on the device wafer. Second, the device feature is through etched by DRIE from the front side. All isolated parts etched in this step remain attached to the wafer by break-off tabs so that they do not fall off. The DRIE etch recipe "MIT69A" was used as developed in the Microsystems Technology Laboratories (MTL) of MIT. The total time taken to etch through the wafer thickness of 300 µm was about 3 hours with a 20 µm halo.

Typical DRIE through etching does not yield an ideal etch at the bottom of the wafer due to footing and a footing radius. The former refers to the eroded silicon structure at the bottom by a reflected plasma attack on the unprotected silicon. The latter refers to the thicker feature size at the bottom due to weakened plasma etching from above. The shallow backside etch effectively alleviates both problems. It prevents the relay contacts from making only point contact along their bottom edge. It also helps increase the fracture strength of the structure by avoiding erosion. Figure 6 shows SEM pictures of the bottom part of three

pieces of silicon. Without the backside etch, (a) has a eroded bottom, (b) has a widened bottom, while (c) has a smooth and straight bottom with the technique of backside etch.

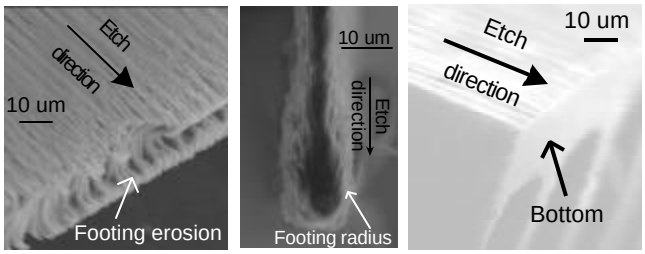

(a) (b) (c)

Figure 6: SEM pictures of DRIE at the wafer bottom.

After the DRIE through etch, it is necessary to remove the Teflon residue from the DRIE process, and also to smooth the sidewalls for better metalization results. To do so, a DRIE isotropic etch using SF_6 for 20 seconds follows the through etch. A half-hour O_2 plasma ashing, a 0.5-μm thermal oxide growth at the temperature of 1100 C, and a BOE striping of oxide follows. A matrix study of these process steps proves they are helpful for better metalization adhesion and contact resistance.

In the third step, a Pyrex handle wafer receives a shallow etch of 50 μm to define pits below the device-wafer components that will move. Fourth, the device wafer is anodically bonded to the handle wafer. Fifth, a shadow wafer is etched by DRIE and is placed on top of the device wafer. The device wafer is sputtered with 100 A of Ti and 1 μm of Au with the shadow wafer acting as a mechanical mask. The shadow wafer is designed so that all sputtered metal on the relay contacts are wired together. This provides a current path for subsequent electroplating. The sputtering machine locates the metal source above the wafer. It does not give metal coverage sufficient for sidewall contacts; our estimation of the average gold thickness on the sidewalls is only 10 % of that on the top wafer surface.

In the sixth step, about 2 μm of copper or gold are electroplated on the device wafer. The copper plating for example is from a commercial acid sulfate solution. Periodic pulse plating with a 5-ms on time and a 1-ms off time is used to improve the uniformity of film thickness and sidewall coverage. The plating was done under constant temperature of 18 C with mild agitation of the plating solution. The current amplitude and plating time is determined by the desired plating thickness and area. In a typical setting, 0.1 A of current lasting for 9 minutes plates 2 μm of Cu on a 10 cm^2 area. After electroplating, thorough rinsing and drying is performed to remove any sulfate from the device to avoid fast oxidation.

After fabrication, the break-off tabs in the device wafer are manually broken to achieve electrical isolation between device features, and the relay is ready for testing. Probes electrically connect the relay. An external source provides pulses for the thermal actuators. Typically, 1-ms pulses with between 50 and 60 Volt amplitudes are required to actuate the relay, which agrees well with our thermal actuator model. Thermal relaxation limits repeated actuation to approximately 5 Hz. Cycle test of 1 Hz actuation have switched the relay 10^5 times, before the metal on the thermal actuator fails. A four-point test is performed to measure the total contact resistance; the best result measured was 60 mΩ with a plated Cu thickness of about 2.5 μm. The same contact carried 3 A of current without contact metal failure.

SUMMARY AND CONCLUSIONS

This paper describes the design, modeling, fabrication and testing of a lateral thermal-actuated bistable MEMS relay for power applications. Its fabrication involves a single DRIE through etch of a silicon wafer. Its current carrying capacity of 3 A and on-state resistance of 60 mΩ is comparable to the best MEMS relays found in literature.

A cantilever is designed to accommodate the effect of fabrication variations on the operation of the bistable double beam and contacts. Transient thermal actuation is employed and a mechanical model for its operation, which includes beam buckling effect, is developed. The model agrees well with FEA and experiment. A method of alleviating the footing and footing radius effects in typical DRIE through etching is developed and presented.

ACKNOWLEDGEMENT

The work reported here was supported by ABB. The authors wish to thank Prof. Martin Schmidt and Jian Li for helpful discussion, and many other MIT MTL members including Kurt Broderick, Dr. Vicky Diadiuk, Gwen Donahue, Ramkumar Krishnan, Paul Tierney, and Dennis Ward for their assistance in fabrication. The corresponding author thanks Prof. Nicolas Hadjiconstantinou of MIT for TA support during the partial course of this work.

REFERENCES

1. Y. Wang et. al, Low-voltage lateral-contact micro relays for RF applications, MEMS '02, 645-648.
2. J. Wong et. al, An electrostatically-actuated MEMS switch for power applications, MEMS '00, 633-638.
3. M. Ruan et. al, Latching micro magnetic relays with multistrip permalloy cantilevers, MEMS '01, 224-227.
4. J. Simon et. al, A liquid-filled microrelay with a moving mercury microdrop, *JMEMS* 6 (1997), 208-216.
5. H. Lee et. al, Electrostatically actuated copper-blade microrelays, *Sensors and Actuators* A 100 (2002), 105-113.
6. W. Taylor et. al, Fully integrated magnetically actuated micromachined relays, *JMEMS* 7 (1998), 181-191.
7. J. Qiu et. al, A centrally-clamped parallel-beam bistable MEMS mechanism, MEMS '01, 353-356.
8. J. Comtois et. al, Characterization of electrothermal actuators and arrays fabricated in a four-level, planarized surface-micromachined polycrystalline silicon process, Transducers '97, 769-772.
9. C. Lott et. al, Modeling the thermal behavior of a surface micromachined linear-displacement thermomechanical microactuator, *Sensors and Actuators* A 101 (2002), 239-250.